GALES, J., ROBERTSON, L., AND BISBY, L. (2016) CREEP OF PRESTRESSING STEELS IN FIRE. FIRE AND MATERIALS. 40, 875–895. DOWNLOAD AT HTTP://ONLINELIBRARY.WILEY.COM/DOI/10.1002/FAM.2345/EPDF

Creep of Prestressing Steels in Fire

John Gales[1], Lucie Robertson[2], and Luke Bisby[3]

[1] Assistant Professor, Carleton University, Ottawa, Canada, john.gales@carleton.ca
[2] Graduate Engineer, Mott MacDonald, Glasgow, United Kingdom, lucie.robertson@mottmac.com
[3] Arup Professor of Fire and Structures, University of Edinburgh, Edinburgh, United Kingdom, luke.bisby@ed.ac.uk

ABSTRACT

When prestressing steel (PS) is applied as continuous unbonded tendons within concrete, as in the case of post-tensioned (PT) construction, localized damage to the tendons may affect the integrity of the entire structure. When fire exposed, unbonded PT concrete structures are prone to tendon rupture due to a complex relaxation and strength reduction relationship influenced by high temperature PS creep. Explicit consideration of creep is necessary for the fire safe design of such buildings. High temperature PS creep has received limited research: few models can be used within the expected service stress range; none reliably model tertiary creep; and no studies are available investigating the influences of metallurgy on high temperature PS creep. A BS 5896 PS creep model is developed and validated. This model is used to provide PS failure insights at high temperatures. This understanding can be used to build validated models of structural fire experiments on PT concrete structural elements and to develop defensible, validated structural models that are essential towards performance based structural fire design of such systems. Finally, the high temperature creep performance of equivalent PS from different mills is compared, demonstrating strong influence of manufacturing and alloying techniques used. Future research is discussed.

Key words: High temperature creep, prestressing steel, optical strain measurement, necking, chemical composition, metallurgy.

Notation

a,*b*,*c*.*d* – empirical creep constants
$\dot{\varepsilon}$ – creep rate (mm/mm per time)
ε – strain (unitless)
$\varepsilon_{cr,o}$ – Primary creep value (unitless)
ε_t – thermal expansion strain (unitless)
ε_{cr} – creep strain (unitless)
f_{pu} – Ultimate strength (MPa)
θ – Temperature compensated time (hours)
σ – Stress (MPa)
t – Time (hours)
T – Temperature (K)
Q – Activation energy (K)
Z – Zener-Hollomon Parameter (hrs-)

1. Introduction

Prestressing steel (PS) is increasingly favoured for reinforcing highly optimized, modern concrete flat slabs owing to various sustainability, economic, and constructability benefits. In the popular construction technique of unbonded post-tensioned (UPT) concrete, prestressing steel is cast inside concrete structural elements in continuous strands or tendons, placed inside lubricated draped ducts which leaves the PS unbonded from the concrete, stressed and anchored only at its ends using special anchors. Whilst highly efficient and effective at ambient temperature, the continuity of UPT steel over multiple bays in a concrete structure can have potential drawbacks – particularly during fire. Localized heating of the prestressing steel, as is likely to occur during real building fires (due to concrete cover spalling, fire compartmentation, travelling fires, ceiling jets, or tendon drape, etc), could result in tendon rupture and would affect slab capacity and integrity distant from the fire [1]. Recent experiments on stressed UPT tendons of realistic length under localized heating have confirmed that thermally-induced rupture can occur at temperatures well below those at which uniformly heated, stressed UPT tendons would fail [2]. The likelihood of rupture of UPT steel tendons at elevated temperature within a concrete structure depends on complex interactions between thermally induced strength reductions and tendon stress variations caused by time, stress, and temperature dependent irrecoverable creep deformations. An accurate and robust method for predicting creep deformation and rupture for any possible transient heating regime is needed to accurately predict the fire resistance of UPT structures.

A computational model for predicting high temperature stress variations in locally-heated unbonded and stressed prestressing steel tendons has previously been developed; this model can reasonably predict observed deformation trends [3][4]. However, this modelling was forced to assume outdated input parameters originating from the 1970s [5], and these were hypothesized as not reflecting the metallurgy or processing of modern prestressing steels, leading to significant overestimation of prestress relaxation [3]. The authors have recently presented new creep model input parameters based on a limited data set and stress range for a specific ASTM A416 prestressing steel, with promising results [6]. However, the prior was not able to provide a creep model that could be used over the full range of relevant stresses due to the inapplicability of the empirically defined model input parameters. The study also discussed the influence of necking on creep failure, but provided no quantified analysis of this. Additionally, the effects of changes in microstructure which occur with increased temperature were not explicitly considered [7], nor were any subtle effects from manufacturing or alloying processes which could have influenced the microstructure of the steel and thereby its performance at high temperature.

This paper represents a logical continuation of the authors' prior work on high temperature creep of prestressing steel. The high temperature deformation behaviour of prestressing steel manufactured in Europe and fabricated according to the BS 5896 standard [8] is tested and analysed in detail; whereas all prior work has been on North American ASTM A416 steel [7][9]. A testing regime using both steady-state and transient thermal uniaxial tensile tests has been undertaken using a novel non-contact optical strain measurement technology based on Digital Image Correlation (DIC) [6]. The current study primarily aims to explore the assumptions used in contemporary creep theory by providing

novel insights into accelerating creep leading to failure – so-called 'Tertiary' creep. A validation exercise for the newly developed creep parameters is presented and the resulting creep model's limitations are discussed.

Available creep parameters for any steel are widely assumed to apply equally to all similar prestressing steels sourced from different manufacturers; however, fabrication and composition differences from producer to producer may influence respective steels' creep responses, particularly at high temperatures and stress levels. This paper therefore considers the creep behaviour of "equivalent" grades of prestressing steel sourced from three separate steel mills: one European (BS 5896 [8]), one North American (ASTM A416 [9]), and one Australasian (AS/NZS 4672 [10]). The creep behaviour of these specific steels is also compared against available results from tests on prestressing steel from the 1970s, fabricated according to ASTM A421 [11], and presented by Harmathy and Stanzak [5]. An exploratory modelling exercise is then undertaken to illustrate the importance of using specific creep parameters for the prestressing steel that is actually being used. The paper concludes with recommendations for future work to improve creep parameters for modelling prestressing steel deformation and rupture in fire.

Defensible performance based structural fire engineering designs of UPT concrete structures require a proper understanding of material response to heating [12][13]. Several high temperature tests on continuous post-tensioned concrete floors were previously performed by the authors [14][15][16]. The tests were densely instrumented and included many complexities of real UPT concrete construction, including a single draped monostrand BS 5896 prestressing strand. The tests revealed highly complex mechanical response to high temperature [15], and the mechanisms responsible for this complexity were shown to be highly dependent on the high temperature stress relaxation of the prestressing steel due to creep. The BS 5896 prestressing steel considered herein is from the same batch used to construct those floor assemblies. The stock also comes from the same mill and identical fabrication processes used in the the Bailey and Ellobody post-tensioned slab test series [17][18]. Accordingly, characterizing the mechanical and creep response of this steel stock is essential to defensibly build structural response models of these heated floor tests, as well as the eventual goal of modelling an entire post-tensioned concrete structure in fire.

2. Creep theory

The current study utilizes the well-known Harmathy creep model [5][19]. This model was chosen so as to provide consistency with previous studies by the authors, and also because it is widely applied in practice [20]. To provide context for the reader, the current state-of-the-art in creep theory, with primary reference to the Harmathy model, is given in this section.

2.1 Background

High temperature creep strain (ε_{cr}) is an irrecoverable deformation that depends on stress, temperature, and time, as well as various micro-structural and metallurgical characteristics. Creep can be observed in tests either using transient (i.e. load the sample to a chosen stress level, maintain the load constant, and then heat at constant rate) or steady state (i.e. heat to

a chosen temperature, then maintain constant temperature and load the sample) test conditions. Tests are typically controlled using constant load, since true stress cannot be directly measured in real time and is therefore 'assumed', sometimes accounting for volumetric changes during testing (more often not). By plotting the measured ε_{cr} (after careful removal of strains due to thermal expansion and mechanical strains due to elastic modulus reduction on heating) a sigmoid (S-shaped) curve can be plotted with respect to a lumped time-temperature parameter that is commonly referred to as 'Temperature Compensated Time', θ. Invoking an empirical coefficient Q, known as the 'activation energy' for creep and measured in degrees Kelvin, θ can be described using an Arrhenius equation as:

$$\theta = \int_0^t e^{-Q/T} dt \qquad [1]$$

where t is the duration, in hours, of an analysis time step [4][20], and T is the temperature in degrees Kelvin. A typical example of an ε_{cr} versus θ curve (i.e. a 'creep curve') for prestressing steel is given in Figure 1(a). The trends in Figure 1 were derived from real test data however the magnitudes have been omitted for illustrative purposes.

The classical creep curve has three distinct phases: (1) a *Primary* phase characterised by a decreasing creep deformation rate and dominated by strain hardening, in which the strain rate progressively decreases as the hardening process increases due to counteraction from dislocations within the grain structure of the steel; (2) a *Secondary* phase described by a 'steady' minimum straining rate, and resulting from the formation and growth of voids (in the form of cavities, pores, and/or cracking) within the grain microstructure; and which (3) eventually causes the straining rate under constant load to accelerate (Figure 1(b)) as 'runaway' strain during a final *Tertiary* phase. The voids are theorized to form along grain boundaries and may be influenced by material impurities, dislocation breakthrough, or distortion of the grains [21]. The acceleration of creep during the Tertiary phase eventually leads to failure [22].

Defining the point of initiation of Tertiary creep is challenging in practice and this issue is uniquely treated in the current paper. The classical definition of the beginning of Tertiary creep is the moment at which the minimum creep rate is observed during the Secondary phase [23]. By determining the minimum creep rate for an ε_{cr} versus θ plot, a Zener-Hollomon parameter, Z, can be derived (in hrs^{-1}) [24]. This may be approximated by determining the slope of the approximately linear Secondary creep phase. A linear tangent to the Secondary phase will intercept the vertical-axis at the so-called Primary creep value, $\varepsilon_{cr,o}$. The extraction of Z and $\varepsilon_{cr,o}$ from a sustained stress uniaxial creep test is illustrated in Figure 1(a). In fire engineering design [20][25] these parameters can be used to predict the amount of creep during the Primary and Secondary creep phases, but *not* during the Tertiary phase. Equation 2 is often used to predict ε_{cr} for steel as:

$$\varepsilon_{cr} = \frac{\varepsilon_{cr,0}}{\ln 2} \cosh^{-1}\left(2^{\frac{Z\theta}{\varepsilon_{cr,0}}}\right) \qquad [2]$$

2.2 Activation energy, *Q*

The advantage of Equations 1 and 2 is that two steady state creep curves at different temperatures and the same loading could overlap with respect to θ [19]. Thus, transient and steady state creep tests at the same loading level can also overlap, as was verified previously in [6]. This idea can be used to advantage if the temperature compensated time reasoning suggested in Equation 1 is valid, since a steady state test can take many hours to complete, whereas a shorter transient test may yield equally useful parameters in a much shorter time. The equivalency of tests should be assured by proper derivation of *Q*, which is an essential parameter in defining θ. Two techniques [22][26] may be used to derive *Q* for a given prestressing steel.

Several creep tests performed at the same load but at different temperatures could be used to derive an accurate value of *Q*. Using this technique, creep strain is plotted against θ, rather than against time, for each test at the same load level. An arbitrary value of *Q* is first chosen for use in Equation 1. This value is then iterated until all creep curves at the same loading coincide with respect to θ. The value of *Q* at which coincidence appears is approximately correct.

A more traditional technique to exactly calculate *Q* is by using a minimum of two steady state creep tests at the same load. Two parameters from each test are needed: (1) the value of the constant creep rate, $\dot{\varepsilon}$, (taken as strain/strain to time) and (2) the temperature, *T*, at which the test was performed, measured in Kelvin. For each test, the natural logarithm of $\dot{\varepsilon}$ and the inverse temperature of the test, *T*, can be plotted and a single value of *Q* can be represented by the slope of this line, thus:

$$\ln(\dot{\varepsilon}) = \ln(A) - (Q)\frac{1}{T} \qquad [3]$$

Where *A* is a constant and represents the intercept with the creep rate axis, but is not needed for the creep modelling performed herein. This method is akin to viewing the deformation characteristics in steel at high temperature as a chemical reaction which takes place at an increasing rate with increasing temperature. Both of these techniques assume that the defined value of *Q* is independent of temperature. It is noteworthy that *Q* depends on metallurgy, which means that if the microstructure of a metal changes the instantaneous activation energy for creep may also be influenced [22].

2.3 Cautions

Various cautions are required when the above creep theory is applied to prestressing steel, all of which were considered when developing the creep parameters and performing the tests described herein:

- **Outdated material parameters may not be applicable to modern materials** – Steel used in older tests may not be representative of contemporary materials. The metallurgical characteristics used in modern steels may differ considerably from those used in the past since, small changes in chemical composition and manufacturing processes may influence creep response. Current design guidance gives creep parameters from the 1970s which may now be outdated [5][20]. Furthermore, creep

parameters are not currently available for the complete stress range expected in a fire situation.

- **The full creep curve must be considered** – The Zener-Hollomon Parameter, *Z*, represents the minimum creep rate and can only be determined with certainty from a full creep curve, including the Tertiary phase. This is particularly important when defining the activation energy for creep *Q*. Current guidance evoking the Harmathy model [20] fails to caution that the *Z* parameter represents a minimum creep rate. Instead it implies that *Z* represents a linear proportionality. Practice has a creep test being halted prematurely resulting in curve fitting of the slope of the first linear region to determine *Z*.
- **Only one set of parameters should be derived from one test** – During a creep test the cross sectional area of a specimen decreases due to Poisson's effect and necking. If the load is increased during a test so that multiple creep parameters can be determined at different stress levels, *Z* may be overestimated since the engineering stress will be less than the true stress. Indeed, Harmathy and Stanzak [5] attempted to derive multiple creep parameters from single tests by adjusting loading mid test, and the creep parameters (where stress was based upon the original cross sectional area), thus overestimating *Z*.
- **Creep equations have traditionally been applied only to Primary and Secondary creep** – Equation 2 is only valid until the transition between Secondary and Tertiary creep phases, since it fails to account for cross sectional area reductions which occur during Tertiary creep [6]. Equation 2 was originally intended for use where 'true' stress changes slowly with time.
- **Creep is influenced by metallurgy which may change with temperature** – The activation energy, *Q*, may actually change in reality, since a specimen may experience metallurgical changes with increases in temperature. Caution is therefore needed if a creep model for prestressing steel is to be used in a transient heating condition. The authors are not aware of any studies (including their own prior work [6]) investigating this issue for prestressing steel temperatures below those considered critical.

3. Methodology

Both ambient and high temperature uniaxial tensile tests were performed to define new creep and mechanical parameters for Grade 1860 MPa prestressing steel. For further test details and methodologies please see Gales et al. [6].

3.1 Materials

This paper focuses on BS 5896 prestressing steel produced in the UK using a blast oxygen furnace process. This steel was used first to develop and verify a Harmathy creep model and compare against other modern prestressing steels, while also providing insights into creep behaviour. To better understand the influence of manufacturing locations and techniques, 'equivalent' prestressing steels from different mills were also considered, including AS/NZS 4672 prestressing steel obtained from Australasia, which was produced in an electric arc furnace, and ASTM A416 prestressing steel from Gales et al. [6], which was produced using a blast oxygen furnace. Test results for historical steel, manufactured

in accordance with ASTM A421 [11], were referenced from Harmathy and Stanzak [5], and these results are also used for comparison to illustrate differing creep responses comparing modern to historical steels. In all cases testing was performed on core wires taken from 7-wire tendons. These were approximately 4.4 mm in diameter and cut to 660 mm in length.

3.2 Testing apparatus

All uniaxial tensile tests were performed using an Instron 600LX testing frame equipped with an environmental chamber for heating specimens up to 625°C under load. The chamber was equipped with a quartz glass viewing window so that strains could be measured optically using DIC. Test specimens were gripped outside the environmental chamber, as shown in Figure 2, with a heated length ratio of 80%. Five K-type thermocouples (with an accuracy of ± 0.0075T with T is measured in ºC) were distributed evenly in the furnace and used to monitor the specimen temperature during testing. Strain measurements were made between two specific thermocouple locations near mid span of heating, and failure of the specimens occurred in this region in most cases. These two thermocouple readings were averaged to define the specimen temperature at the location of strain measurement. An optical non-contact DIC measurement technique was applied using a digital single lens reflex (DSLR) camera and the GeoPIV8 DIC code [27].

3.3 Testing regimes

Various uniaxial tensile testing regimes were used. These included:

(1) **Steady state creep tests –** wherein the specimen was heated to a predefined target temperature, strain was measured while load was increased up to a sustained target stress, and load was then held constant until failure.
(2) **Transient creep tests –** in which the specimens were loaded initially to a target load (stress) at ambient temperature, and strain was then measured while the specimens were heated at a uniform ramp rate until failure.
(3) **Thermal expansion tests** – following the same procedure as for transient creep tests, however with zero loading and heating to a pre-defined temperature.
(4) **Stress relaxation tests** – in which specimens were loaded initially to a target stress level at ambient temperature, and then fully restrained and heated using a pre-defined heating curve for a fixed duration.
(5) **Tensile strength tests –** which were heated without any applied load up to a fixed temperature and then tested to failure under crosshead displacement control.

All tests that required pre-heating for steady state conditions were soaked at the relevant target temperature for 15 minutes to ensure uniform specimen temperature. Fifteen minutes was chosen on the basis of tests in which a prestressing steel wire was heated to 500ºC while monitoring thermal expansion and it was noted that no additional thermal expansion was measurable after 15 minutes. Post-test analysis using DIC allowed the total strain to be determined; mechanical and thermal strains were then isolated and subtracted to estimate the creep strain. Table 1(a-c) provides an overview of the nearly 70 individual tests that were performed, including: the type of test, heating rate, and loading rate.

Validation of the experimental and DIC techniques for deformation measurement at high temperature is given elsewhere [6].

3.4 Micro-structural analysis

For each prestressing steel type, unrestrained and unloaded wires were heated to temperatures of 200, 400, 500, 600, 700 and 800ºC, respectively, using an annealing oven a temperature ramp rate of 10°C/min. Four thermocouples were used to monitor the gas and sample temperatures. The wires were held at the target temperature for 1.5 hours before being cooled slowly in air. A small section was cut from each wire and mounted in EpoxiCure resin. These were then ground using gradually finer grit paper and then polished with diamond paste to obtain a flat, scratch-free surface. The samples were then etched with 2% Nital solution to expose their grain structure. The microstructure of the samples was examined using a Zeiss Axioscope light microscope following a procedure outlined in Robertson et al. [7].

4. High temperature characterization for prestressing steel

Using the creep theory described above, DIC results are used in the following sections to show high temperature creep deformation trends and material input parameters (Q, Z, $\varepsilon_{cr,o}$) for modelling modern (BS 5896) prestressing steel at high temperature. Other prestressing steels are considered in Section 5.

4.1 Separating creep strain from total strain

A steady-state creep test may take days to complete under certain conditions, and because creep can occur during loading, the true quantity of creep occurring in a test may be poorly estimated [20][28]. In a transient creep test, mechanical strain can be approximately quantified. Creep strain can be determined by subtracting strain from thermal expansion and additional strains that occur with elastic modulus reductions at temperature increases. However, as temperature increases the steel yield strength also decreases and becomes intertwined with creep; this causes classical definitions of these distinct classes of strains to lose their meaning [6].

In the current study, creep is approximated by the separation of thermal and mechanical (elastic and plastic) strains. Thermal strains can be predicted by performing transient heating tests under zero load. When comparing an unloaded thermal relaxation test of BS 5896 prestressing steel against the predictions of EN 1992-1-2 [29] (Equation 4), a negligible (0.13%) strain difference was observed at 500ºC.

$$\varepsilon_t = -2.016\times10^{-4} + 10^{-5}\,T + 0.4\times10^{-8}\,T^2 \quad \text{for } 20^{\circ}\text{C} < T < 1200^{\circ}\text{C} \qquad [4]$$

It is therefore assumed herein that Equation 4 can be used to isolate creep strains. By calculating the additional mechanical strain occurring due to elastic modulus reductions during each measurement interval during heating, plastic strains can be approximately determined. The EN 1992-1-2 [29] equations for elastic modulus reduction were utilized to perform these adjustments in the current work. Whilst these equations presumably

implicitly include some creep the EN 1992-1-2 [29] values were observed to correlate with values observed in the mechanical testing described below.

4.2 Steady state and transient creep tests

Creep parameters can be extracted from the creep curves curve produced from creep tests, as described earlier. Transient creep tests can better represent conditions during a real fire, and given that these tests can be performed quickly, creep parameters for prestressing steel at different stress levels can also be produced with fewer tests.

4.2.1 Activation energy for creep

To plot ε_{cr} versus θ correctly, Q in Equation 3 must be determined. This requires careful measurement of creep strains under various stress and temperature conditions. The activation energy for creep, Q, is physically the energy needed to cause movement of atoms (dislocation and/or slip of the grain structure) from one stable state to a new one. The value of Q has real physical meaning, although it can easily be mistaken as simply an empirical correction factor and this can produce erroneous ε_{cr} versus θ plots that are fundamentally flawed.

Four creep tests at steady state temperatures were performed at 410ºC, 427ºC (repeated for verification), and 440ºC, all at a load equivalent to an initial stress of 700 MPa. Taking the minimum creep rate with respect to time and applying Equation 3 gives Q as 37200K with correlation coefficient $R^2 = 1.00$. This was verified by equating transient tests (1ºC/min to 10ºC/min) with respect θ at 927 MPa.

Since Q depends on the microstructure of the steel it may also change with temperature. The authors have found that within the tested stress and temperature ranges used herein the derived creep parameters appear to be satisfactory (see Section 4.5). Furthermore, since the available guidance typically restricts the stress ranges over which prestressing steels can be used in service, only creep tests within this range (<500ºC and <1300 MPa sustained stress) have previously been considered. The data set used to define Q should be expanded to determine the sensitivity of the values extrapolated from the available tests.

4.2.3 Creep parameters

Table 1(a) summarizes the test conditions used to characterize the BS 5896 prestressing steel's high temperature material response. Creep tests were performed at stress levels between 200 MPa and 1664 MPa at temperatures below 500ºC. Expressions were then developed to describe creep parameter variation with respect to applied stress, σ. The resulting expressions for creep parameters for BS 5896 prestressing steel (for insertion into the Harmathy [5] model) developed are:

$$Z = ae^{b\sigma} = 1.02x10^{16} e^{0.019\sigma} \qquad 687 \text{ MPa} < \sigma < 1300 \text{ MPa} \qquad [5a]$$

$$Z = 0.7x10^{8}\sigma^{5} \qquad 200 \text{ MPa} < \sigma < 687 \text{ MPa} \qquad [5b]$$

$$\varepsilon_{cr,0} = c\sigma^{d} = 1.072x10^{-7}\sigma^{1.645} \qquad [5c]$$

where the units of σ are MPa and Z are in hrs^{-1}. Equations 5 (a-c) take the same form as suggested by Harmathy and Stanzak [5] for Z, and $\varepsilon_{cr,o}$, only with new values for empirical constants *a, b, c,* and *d*. These coefficients were defined based on non-linear least-squares empirical regressions. The equations above are strictly only valid with Q = 37200K and for the stated stress ranges for this specific batch of prestressing steel. The Primary creep variable was derived from poorly reproducible (however small) values. Both steady state and transient tests were used to construct these equations. Figures 3(a) and 3(b) show the raw data used to develop Equations 5a-c.

4.3 Tertiary creep behaviour

Equation 2 is traditionally assumed as being valid only to predict Primary and Secondary creep; it was not developed for Tertiary creep, yet it assumes that knowledge of the creep developed during the Secondary phase is sufficient to define failure [5][30]. Revisiting Figure 1, which is based on a real creep test of prestressing steel but with magnitudes removed for clarity of illustration, the cross-sectional area reduction due to necking during Tertiary creep can be calculated *a posteriori* using DIC; the onset is taken herein as the instant when necking appears within the DIC camera's field of view. The reduction in cross-sectional area for this figure was determined at the precise position of necking and at another location arbitrarily chosen away from the position of necking.

Figure 1 shows the creep curve (ε_{cr} versus θ) and cross-sectional area reduction at these two locations for a typical test. Gales et al. [6] previously hypothesized that Tertiary creep depends on both reductions in material properties *and* changes in the geometry; this simply being the engineering strain manifestation of necking. In the current study the authors hypothesize, using the measured reduced cross-sectional area, that Equation 2 can be compensated to account for the measured area reduction; and therefore to compensate for the true stress (provided this changes sufficiently slowly). Two creep tests on BS 5896 steel are used to illustrate this idea. The first is a steady state test performed at 647 MPa initial stress and 440ºC. Equation 2 was extrapolated with the appropriate Z, and $\varepsilon_{cr,o}$ values (which would be applicable for true stress). Figure 4 shows the predicted true stress compensated creep curve, as well as the prediction without compensation. It is clear that Equation 2 is able to closely predict creep strains provided that the true stress is estimated correctly based on the necking area *a posteriori*. A second, more complicated transient test can also be considered and is also shown in Figure 4. In this case thermal dilation effects are present which must also be separated. Figure 4 shows the predicted responses; again the model matches the trends, however with obvious scatter most likely due to the sensitivity associated with measuring such small displacement and/or the rapid changes in area (and hence true stress).

Two additional plots are also shown which help to validate this hypothesis while also demonstrating good repeatability between tests. Figure 5 shows predictions and results for two transient creep tests at 927 MPa with the compensated model prediction shown. Figure 6 shows two steady state tests at 647 MPa. All predictions compare well, with similar error as in Figure 4 (<15% difference between modelled and experimental strain) and considerable improvements in the accuracy compared to the model without area

reduction. These data support the hypothesis that the Harmathy model can be extended for use in the tertiary creep phase, albeit only once the area reduction is known.

The above suggests a need to perform additional research to study Tertiary creep and to define an *a priori* Tertiary creep model without the need to measure the necking before Tertiary creep can be predicted; this is an ultimate goal for failure analysis of UPT concrete structures in fire. The following issues also need to be addressed in future research:

- By considering the point at which specimens 'neck' in the Tertiary phase and the strains in this region, it appears possible to model Tertiary creep. However, if specimen area is taken away from the necking region and used to quantify true stress the model is unable to predict the Tertiary creep deformation. This suggests that any accurate model for Tertiary creep must consider volumetric changes near failure.
- A more thorough investigation into the sensitivity of the creep equations in modelling Tertiary creep is needed since stresses increase exponentially during this phase. The creep model was only intended for use when true stress changes relatively slowly.
- The volumetric changes observed during Tertiary creep require better understanding. On the macro-scale Tertiary creep can be distinguished by physically observing localized necking. On the micro-scale it is evident that micro-cavities and void formations play roles.

4.4 Mechanical Behaviour

To provide some insight into failure, mechanical tests to failure were performed at various steady-state temperatures. The strength relationship with temperature obtained for the BS 5896 steel is shown in Figure 7 (loading rate of 2 mm/min). An average ultimate strength (f_{pu}) at ambient temperature of 2033 ± 11 MPa was obtained, with strength reductions observed at 100ºC intervals up to 500ºC. Temperatures greater than 500ºC were not considered, since prestressing steel would rarely be relied on at such high temperatures in design. High temperature strength tests were repeated twice, showing good repeatability. The true stresses shown in the figures are based on DIC measurements of reduced cross-sectional areas. It is clear that true stress increases drastically approaching failure, in much the same way as during Tertiary creep. Figure 8 shows the observed strength reductions along with those suggested in EN 1992-1-2 [29]. These are based on engineering stress rather than true stress. Nonetheless, Figure 8 shows that the strength reduction of the BS 5896 steel follows the expected behaviour, with nearly 50% tensile stress loss at temperatures below 400ºC.

Design code guidance rarely states the rates used in tests (loading or heating rates) to develop high temperature material property reduction factors. These rates can, however, be expected to influence the results obtained since failure is inevitably influenced to more or lesser degree by time-dependent creep. In the steady-state strength tests undertaken for the current project, a crosshead speed of 2 mm/min was chosen. Had a different displacement rate been used, say 1 mm/min, the high temperature f_{pu} values would have been different, resulting in different reduction factors (this was seen when a second 500ºC test was performed at 1 mm/min and the corresponding high temperature f_{pu} was 12% lower

than in tests performed at 2 mm/min). Loading and heating rates should therefore be reported when high temperature tensile test results presented.

Two additional observations are noteworthy in Figure 8: first, the predominant heating rate used for transient creep tests (2ºC/min) appears to agree well with material property reduction factors given in [29], as does the displacement rate of 2 mm/min; and second, depending on the time of heating and load scenario it is possible to fail the prestressing steel below the EN 1992-1-2 temperature definition of failure. Additional research into failure of prestressing steel at high temperature is warranted so that Tertiary creep and mechanical failures can be accurately distinguished and predicted.

4.5 Validation

A validation exercise was performed to confirm that the BS 5896 prestressing steel creep parameters developed herein could be satisfactorily used to predict Primary and Secondary creep response. The new parameters given in Equation 5 were used in conjunction with the stress relaxation computational code described by Gales et al. [4], which also uses Equation 2 for predicting and modelling creep.

The aforementioned Instron 600LX testing frame and environmental chamber were used to conduct two stress relaxation tests of BS 5896 prestressing steel to provide raw data for modelling purposes. Using the heat transfer model described in Bisby and Kodur [32], the environmental chamber was programmed to simulate the heating exposure for prestressing steel embedded in a semi-infinite concrete slab and exposed to an ASTM E119 standard fire from below [33]. Two transient heating scenarios were used, representing predicted heat transfer behaviour for prestressing steel at two concrete cover axis distances, namely 28 mm and 35 mm. These axis distances represent typical covers required to achieve fire resistance ratings of 120 minutes in the International Building Code [34] and EN 1992-1-2 [29], respectively, for ‘continuous’ construction. Five thermocouples (TCs) were used to characterize the longitudinal profile of temperature of the prestressing steel for modelling purposes. One TC was placed on the bottom on the environmental chamber on the prestressing steel, three TCs were equally placed inside the chamber on the prestressing steel, and one TC was placed on the prestressing steel just outside the top port of the chamber. The test began at an initial stress level of 1200 MPa (as might be typical for UPT prestressing steel in a building in practice). The grips were locked in place and the steel was allowed to relax by thermal deformation and creep.

Figure 9 illustrates the stress relaxation from both tests, along with the predictions using the computational code [4]; the peak temperature of the prestressing steel is also given. Less than 50 MPa difference between the predictions and the tests was observed, thus verifying the new creep parameters.

5. Creep response

In practice, the available creep parameters for prestressing steel are widely assumed to apply to all grades sourced from internationally. However, manufacturing and microstructural differences may influence creep deformations at high temperature. This section compares the creep response of “equivalent” grades of prestressing steel sourced from different locations internationally.

5.1 Creep parameters for other prestressing steels

Table 1 describes the tests performed for each of the prestressing steels. Where possible the testing regime was the same as for the BS 5896 prestressing steel discussed above, and the general observations already made regarding repeatability, steady state versus transient testing equivalence, and increases in Z with increases in load level all hold equally. However, the activation energies for creep, Q, for each specific prestressing steel were considerably different. As the supply of each specific steel was limited, Q for the ASTM A416 steel was approximated in this study as 23000K based on equating two transient creep tests at the same load level but different heating rate. The AS/NZS 4672 steel Q value was derived from Equation 3 using steady state tests, giving Q = 34350K. Equations 6 and 7 were derived based on an $R^2 > 0.99$ fit with respect to minimum creep rate, Z. These equations should only be used with the activation energies noted above.

NZS 4672 prestressing steel

$$Z = ae^{b\sigma} = 4.37x10^{14}e^{0.015\sigma} \qquad 700 \text{ MPa} < \sigma < 1200 \text{ MPa} \qquad [6a]$$

$$\varepsilon_{cr,0} = c\sigma^{d} = 1.15x10^{-11}\sigma^{2.72} \qquad [6b]$$

ASTM A416 prestressing steel

$$Z = ae^{b\sigma} = 2.5x10^{8}e^{0.0145\sigma} \qquad 690 \text{ MPa} < \sigma < 1000 \text{ MPa} \qquad [7a]$$

$$\varepsilon_{cr,0} = c\sigma^{d} = 4.1x10^{-7}\sigma^{1.2} \qquad [7b]$$

The previous equations derived by Harmathy [5], with an activation energy of 30550K for ASTM A421 [11] prestressing steel are:

$$Z = ae^{b\sigma} = 8.21x10^{13}e^{0.0145\sigma} \qquad 172 < \sigma < 690 \text{ MPa} \qquad [8a]$$

$$\varepsilon_{cr,0} = c\sigma^{d} = 9.26x10^{-5}\sigma^{0.67} \qquad [8b]$$

Equations 6 through 8 clearly show that each of these nominally identical prestressing steels has considerably different derived creep parameters.

5.2 Prestressing steel comparison

Three additional test series were undertaken to more thoroughly compare the different prestressing steels:

(1) **Comparative creep tests** – a creep test was performed for each steel at 427ºC at approximately 35% of the ambient f_{pu}. This allowed the creep response of all three modern prestressing steel to be compared experimentally for a single, representative load case. Strength tests were also performed for the AS/NZS 4672 steel for comparison with the BS 5896 steel, considering both strength and elastic modulus.

(2) **Microstructural analysis** – all three steels were compared at the microstructural level (at 100X magnification). Grain structures at ambient and after exposure to steady state heating were compared for each.

(3) **Numerical comparisons** – a numerical modelling exercise was performed to construct predicted creep response curves for each of the steels for a simulated creep test using

specific creep parameters in comparison to those proposed by Harmathy and Stanzak [5] or currently suggested in the literature [20].

5.2.1 Comparative creep tests

Steady state creep tests were conducted at 427ºC (chosen as the assumed critical temperature [34]) at an approximate initial stress (constant load) of 35% of f_{pu} (about 700MPa). Repeat test were also performed for BS 5896 and AS/NZS 4672 steels. It was not possible to perform a repeat test for the ASTM A416 steel due to a limited of supply of this material. The full creep curves (Figure 10) and the normalized creep rates were compared (Figure 11).

Figure 10 gives the strain versus time results for one creep test for each steel, and shows that the AS/NZS steel exhibited the least creep, whereas the BS 5896 steel exhibited the most. This confirms that nominally identical steels may display significantly different creep behaviour, and that this must be accounted for in analyses where creep plays an important role (as in tendon rupture predictive modelling).

Figure 11 illustrates the normalized time (the total test time divided by its duration) with respect to creep rate (with the creep rate determined with respect to each 10% normalized time interval) for both the BS 5896 and AS/NZS 4672 steels; repeat tests are included. The AS/NZS steel exhibited a lower creep rate than BS 5896 steel. Both AS/NZS steel tests lasted for more than 5 hours before failure, whereas the BS 5896 steel tests lasted less than 1.2 hours until failure and the ASTM A416 lasted 1.4 hours. The AS/NZS steel thus exhibits higher creep resistance (about 4 times in terms of duration at this load and temperature) than ‘equivalent’ steels from elsewhere. The current comparison and results are only for a single stress level; additional research in this area is warranted.

Figure 12 shows a comparison of the strength of BS 5896 and AS/NZS 4672 steels. Despite yielding equivalent performance at ambient temperature, as expected, the AS/NZS 4672 steel shows obviously greater strength at elevated temperature when compared to the BS 5896 steel. At 400ºC the BS 5896 steel has an ultimate strength of 965 MPa, whereas the AS/NZS 4672 specimen has a strength of 1079 MPa. The AS/NZS 4672 steel also shows lower ultimate strain at higher temperatures in comparison to BS 5896. AS/NZS 4672 showed similar retained elastic modulus as BS 5896.

The high temperature performance of the prestressing steels may be partly explained by their histories of manufacture, specific alloying, and chemical composition. Table 2 shows the composition of the prestressing steels used in this study, demonstrating clear differences in material composition between the steels. Mill certificates for each steel indicated the proportions of only Carbon, Manganese, Phosphorous, Silicon and Sulphur, with each being reasonably similar on this basis. Table 2 shows that the steels are subtly different. For example, the addition of higher chromium and lower sulphur content in the AS/NZS steel, which was manufactured using an electric arc furnace. Chromium is typically alloyed to improve resistance to corrosion, but is also known to improve retention of mechanical properties at high temperature [35]; this improvement for prestressing steel behaviour in fire with additional chromium has not previously been studied to the knowledge of the authors. The specimens with higher sulphur contents suggest blast furnace manufacturing. Since all prestressing steels tested herein were sourced from

different mills and fabricated in different countries, since the manufacture of prestressing steel is known to affect the creep response at ambient temperature [36], and since creep accelerates at elevated temperature, the manufacturing and alloying history can at least partly explain the different high temperature creep responses. Differences in AZS/NZ 4672 steel led to a strength increase at high temperature of at least 10% for every temperature considered, and to a four fold increase in creep times observed at temperatures considered critical (427°C) in fire under realistic stress levels (700MPa). It is therefore clear that the creep performance of prestressing steel in fire can neither be assumed on the basis of the available creep parameters, nor on the basis of mill certificates alone.

5.2.2 Microstructural analysis

The microstructural characteristics of the AS/NZS 4672 and BS 5896 steels before and after high temperature exposure were considered. Additional micro-structural analysis of prestressing steel wires (ASTM A416 steel) was previously undertaken by MacLean [37][38] and is included for comparison. The Micro-structural analysis is of particular importance with respect to the stability of the prestressing steel's microstructure – an assumption that could lend credence to the use of a constant Q for the transient temperature ranges used in this paper.

Figures 13 to 15 show micro-structural images for wires at ambient temperature and after exposure to 500ºC and 700ºC, respectively, for longitudinal sections. Sections from both unheated prestressing wires and those heated below 500ºC exhibited long, well defined grains running parallel across the field of view. These grains are a result of the cold drawing manufacturing process. Pearlitic banding is also evident. This pearlitic banding disappears after exposure to temperatures above 500ºC. Steel heated to 500°C and 600°C exhibited a finer grain structure, having less well-defined longitudinal grains. Pearlitic bands began to dissociate into ferrite and globular iron carbide. By 700ºC the directionality of the grain structure is lost. Each prestressing steel wire exhibited similar trends at each temperature. Each structure appeared micro-structurally stable below temperatures of 500ºC. This supports use of the creep parameters applied in the current study, since all testing was performed below 500ºC. Above 500ºC microstructure changes can be expected and parameters (such as Q) may be influenced, thus affecting the validity of the creep theory presented herein.

5.2.3 Predictive numerical modelling

Two numerical modelling predictions were made to compare modern and older creep parameters (for Primary and Secondary creep only) using equations 1 and 2. This illustrative comparison is intended to show that the creep model developed for each prestressing steel predict different levels of creep behaviour under the same loading and heating conditions. The modelling results are a compilation of preceding creep parameter equations (equations 6 to 8) used in conjunction with Equation 2. A first comparison (Figure 16) considers a steady state temperature of 350ºC and loads of 700 and 1000 MPa. A second comparison (also shown in Figure 16) considers loading of 700 MPa and two steady state temperatures of 350ºC and 427ºC. In both comparisons, the predictions suggest that the older prestressing steel would experience the highest creep losses, whereas the

AS/NZS steel would exhibit the lowest. This again emphasizes that creep parameters should strictly only be used with the steel for which they were developed.

6 Recommendations

There are two main reasons that a designer may need to estimate creep of a prestressing steel at elevated temperatures: (1) to evaluate the potential for prestress relaxation and the possible consequences for overall structural performance – *where maximum tendon stress losses are desired*, and (2) to conservatively predict prestressing steel rupture – *where minimum tendon stress losses are desired*. In the event that an estimate of stress relaxation of prestressing steel is needed to consider fire-degraded shear and flexural capacities of a UPT concrete slab (which rely on the in-service stress level for capacity estimation), the creep parameters derived for the BS 5896 prestressing steel could be considered. These parameters can be used for the full service stress range, and will predict more conservative relaxation than the parameters derived for other modern prestressing steels in the event that the prestressing tendons do not rupture during fire. However, if a designer needs to predict the earliest stress-strength interception (in the absence of more research into Tertiary creep and mechanical failure) to predict premature tendon rupture, the AS/NZS parameters could be considered since they will yield a conservative prediction.

In the absence of a statistical study of multiple mill prestressing steels analyzed for high temperature performance, the authors recommend that designers requiring accurate creep information should develop their own high temperature creep parameters for specific prestressing steels. A reasonably limited suite of creep tests may be used to determine new material input parameters. The minimum number of necessary tests, based on the work presented in the current paper, is five. These tests would include two steady state creep tests at the same stress level, but different temperature, and would be used to derive Q, which can be used to relate time and temperature effects. The chosen stress level should be between the upper stress level in the expected in-service stress (i.e., about 1200 MPa) and a lower stress level that the designer would tolerate in the event of high temperature exposure. This lower bound value may represent the stress loss needed to cause a flexural or shear failure of the element. The temperatures of these tests must also adhere to three additional criteria: (1) they should be below 500ºC for prestressing steel; (2) two different temperatures should be chosen; and (3) the temperatures in conjunction with the stress level should not cause mechanical yielding before the constant load level is reached. The last point is necessary to produce θ-ε_{cr} creep curves with minimal influences from mechanical damage at the beginning of the test. EN 1992-1-2 [29] could be used in the absence of new tensile strength tests. A minimum of three transient tests at different service stress levels (within the aforementioned stress range), including one stress level equal to one of the two steady state tests noted above are also needed. It would be preferable to conduct as many transient tests as possible, at different loads, to accurately characterise the behaviour of the steel at all relevant stress levels. A repeat transient test at the same sustained stress level as the steady state test could also be performed to verify the activation energy.

7 Conclusions

This research presented herein has provided a number of novel insights and recommendations regarding creep in prestressing steel. These are summarized as follows:

- High temperature Primary and Secondary creep parameters have been developed and validated and can be used to model creep deformation of a specific BS 5896 prestressing steel over the full credible in-service stress range.
- Microscopic study of the three prestressing steels tested herein indicated no observable microstructural changes with increasing temperature below 500^{o}C. This supports use of transient creep tests as a means of deriving creep parameters for prestressing steels and the use of creep models under transient temperature regimes.
- Chemical analysis of the three prestressing steels indicated distinct manufacturing differences for seemingly equivalent prestressing steels that clearly affect high temperature creep and strength behaviour. Current guidance fails to highlight variability between different steels despite the influence on high temperature behaviour.
- Guidance has been given for development of case-specific creep parameters other than those already available. This allows for relatively rapid and economic development of creep parameters with a minimum suite of five creep tests.
- Valuable material behaviour information has been provided that can be used to build validated numerical models of structural fire experiments on prestressed and post-tensioned concrete structural elements, and to develop defensible structural fire models; these are essential to advance towards performance based structural fire engineering design.
- Results showed that existing creep models can be compensated to consider the 'volumetric' changes associated with Tertiary creep behaviour. However additional research is needed to model Tertiary creep *a priori*. Accurate modelling of Tertiary creep requires the underlying mechanisms causing necking behaviour of the specimen at high temperature to be better understood. It has been demonstrated that optical strain measurement can be used to provide the requisite data for this work.
- Despite all prestressing steel specimens having essentially equivalent mechanical characteristics at ambient temperature, their behaviour at high temperature differed considerably. Where consideration of creep is known to be important for predicting structural response (and failure), creep parameters should therefore strictly only be used with the specific prestressing steel for which they were developed.

Acknowledgements

The authors would like to acknowledge the contributions of Dr Andy Take, Zuzana Dudorova, Dr Jane Blackford, Kevin MacLean, Ryan Haick, and Dr Andrew Buchanan. We gratefully acknowledge the support of the Ove Arup Foundation, the UK Royal Academy of Engineering, the Natural Sciences and Engineering Research Council of Canada, and Bridon Steel.

References

[1] Gales, J., Bisby, L., and Gillie, M. Unbonded Post Tensioned Concrete in Fire: A Review of Data from Furnace Tests and Real Fires. *Fire Safety Journal*. 2011; **46** (4):151-163.

[2] Gales, J., Bisby, L., and Gillie, M. Unbonded Post Tensioned Concrete Slabs in Fire – Part I – Experimental Response of Unbonded Tendons under Transient Localized Heating. *Journal of Structural Fire Engineering*.2011; **2** (3):139-154.

[3] Gales, J., Bisby, L., and Gillie, M. Unbonded Post Tensioned Concrete Slabs in Fire – Part II – Modelling Tendon Response and the Consequences of Localized Heating. *Journal of Structural Fire Engineering*. 2011; **2**(3):155-172.

[4] Gales, J., Bisby, L., MacDougall, C., and MacLean, K. Transient High-Temperature Stress Relaxation of Prestressing Tendons in Unbonded Construction. *Fire Safety Journal*, 2009; **44**, 570-579.

[5] Harmathy, TZ., and Stanzak, W. Elevated-Temperature Tensile and Creep Properties of Some Structural and Prestressing Steels. *Fire Test Performance ASTM Special Technical Publication 464*, ASTM, Philadelphia Pa, 1970. 186-207.

[6] Gales, J., Bisby, L., and Stratford, T. New Parameters to Describe High Temperature Deformation of Prestressing Steel Determined using Digital Image Correlation. *Structural Engineering International*. 2012; **22**(4): 476-486.

[7] Roberston, L., Dudorova, Z., Gales, J., Vega, E., Stratford, T., Smith, H., Blackford, J., and Bisby, L. Micro-structural and Mechanical Characterization of Post-tensioning Tendons Following Elevated Temperature Exposure. *Applications of Structural Engineering Conference*, Prague, CZ, 2013; 474-479.

[8] BSi. Specification for High Tensile Steel Wire and Strands for the Prestressing of Concrete, BS 5896-12. 2012. British Standards Institution, London.

[9] ASTM A416. Standard Specification for Steel Strand, Uncoated Seven-Wire for Prestressed Concrete. *Rep. No. A416 / A416M-01,* American Society for Testing and Materials, West Conshohocken, PA. 2003.

[10] AS/NZS 4672. Prestressing Strand Standard 4672. Standards Australia New Zealand, Wellington, NZ. 2007.

[11] ASTM A421. Standard Specification for Uncoated Stress- Relieved Steel Wire for Prestressed Concrete. *Rep. No. A421 / A421M-01,* American Society for Testing and Materials, West Conshohocken, PA. 1965.

[12] Harmathy, TZ., and Lie, TT. Fire Test Standard in the Light of Fire Research. *ASTM STP 464*, 85-97.

[13] Bisby, L., Mostafaei, H., Pimienta, P. State of the Art on Fire Resistance of Concrete Structures: Structure-Fire Model Validation. In NIST-Special Publications: International R&D Road Map for Fire Resistance of Structures. 2014. 26pp. *In press.*

[14] Gales, J., Bisby, L., Stratford, T., Krajcovic, M. Tests of continuous post-tensioned concrete slabs under localized fires. Interflam 2013:13th International Conference and Exhibition on Fire Science and Engineering. Royal Holloway College. 1131-1142.

[15] Gales, J., Bisby L. Deformation and response of continuous and restrained post-tensioned concrete slabs at high temperatures. Proceedings of the 8th International Conference on Structures in Fire. Shanghai, China. 305-312.

[16] Gales, J. Unbonded Post-tensioned Concrete Structures in Fire. PhD thesis. University of Edinburgh. 2013. 348pp.

[17] Bailey, CG., and Ellobody, E. Comparison of Unbonded and Bonded Post-Tensioned Concrete Slabs under Fire Conditions. *The Structural Engineer*. October 2009; **87** (19), 23-31.

[18] Bailey, CG., and Ellobody, E. Fire Tests on Unbonded Post-Tensioned One-way Concrete Slabs. *Magazine of Concrete Research*. 2009; **61** (1), 67-76.

[19] Harmathy, TZ. Comprehensive Creep Model. *Transactions of the ASME Journal of Basic Engineering*, 1967; **89**(3): 496-502.

[20] Purkiss, JA., and Li, Y. Fire Safety Engineering Design of Structures. BH, London, UK. 2013.

[21] Yao, H., Xuan, F., Wang, Z., and Tu, S. A Review of Creep Analysis and Design under Multi-axial Stress States. *Nuclear Engineering and Design*, 2007; **237**, 1969-1986.

[22] Smith, W. Principals of Material Science and Engineering. McGraw Hill, NY. 1996.

[23] Williams, SJ., Bache, MR., and Wilshire, B. Recent Developments in Analysis of High Temperature Creep and Creep Fracture Behaviour. *Materials Science and technology.* 2010*;* **26** (11), 1332-1337.

[24] Zener, C., and Hollomon J. Effect of Strain Rate upon Plastic Flow of Steel. *Journal of Applied Physics*, 1944; 15-22.

[25] Harmathy, T.Z. Properties of Building Materials. *The SFPE Handbook of Fire Protection Engineering*. 1988; 378-391.

[26] Lewinsohn, CA., Bakis, CE., Tressler, RE. Methods of Determining the Temperature Dependence of Primary Creep. *Fiber, Matrix, and Interface properties ASTM STP 1290*, 1996; 9-18.

[27] White, DJ., Take, WA., Bolton, MD. Soil Deformation Measurement Using Particle Image Velocimetry (PIV) and Photogrammetry. *Geotechnique*. 2003; **53**(7), 619-631.

[28] Holdsworth, S. Advances in Assessment of Creep Data during the Past 100 years. *Transactions of the Indian Institute of Metals*. 2010; **63** (2-3), 93-99.

[29] CEN. Eurocode 2: Design of Concrete Structures, Parts 1-2: General rules-Structural fire design, EN 1992-1-2. European Committee for standardization, Brussels. 2004.

[30] Williams-Leir, G. Creep of Structural Steel in Fire: Analytical Expressions. *Fire and Materials*. 1983; **7**(2), 73-78.

[31] Gales, J. Transient High-temperature Prestress Relaxation of Unbonded Prestressing Tendons for Use in Concrete Slabs. *M.Sc. Thesis*, Department of Civil Engineering, Queen's University, Kingston, On, Canada. 2009; 197 pp.

[32] Bisby, L., and Kodur, V. Evaluation of Fire Endurance of Concrete Slabs Reinforced with Fiber Reinforced Polymer Bars. *ASCE Journal of Structural Engineering*. 2005; **131**(1), 34-43.

[33] ASTM E119. Test Method E119-12: Standard Methods of Fire Test of Building Construction and Materials" *Rep. No. E119-12*, American Society for Testing and Materials, West Conshohocken, PA 2012.

[34] IBC. International Building Code. International Code Council, USA. 2012.

[35] Malouk, M, and Zaniewski Z. Materials for Civil and Construction Engineers. 3rd edition, Pearson, 2011; 582 pp.

[36] Clark, N., and Walley, T. Creep of High Tensile Steel Wire. *ICE Proceedings*. 1953; **2**(2). 107-154.

[37] MacLean K. Post-fire Assessment of Unbonded Post-tensioned Concrete slabs: Strand Deterioration and Prestress Loss. *M.Sc Thesis*, Department of Civil Engineering, Queen's University, Kingston, ON, Canada. 2007.

[38] MacLean, K., Bisby, LA., and MacDougall, CC. Post-fire Assessment of Unbonded Post-tensioned Slabs: Strand Deterioration and Prestress Loss. *ACI-SP 255: Designing Concrete Structures for Fire Safety*, American Concrete Institute, 2008; 10 pp.

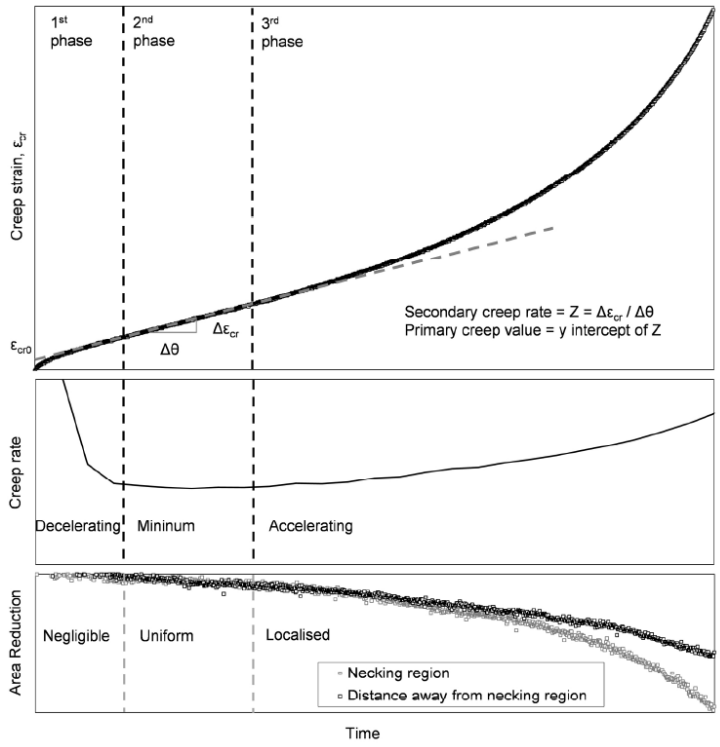

Figure 1: Creep theory applied to prestressing steel.

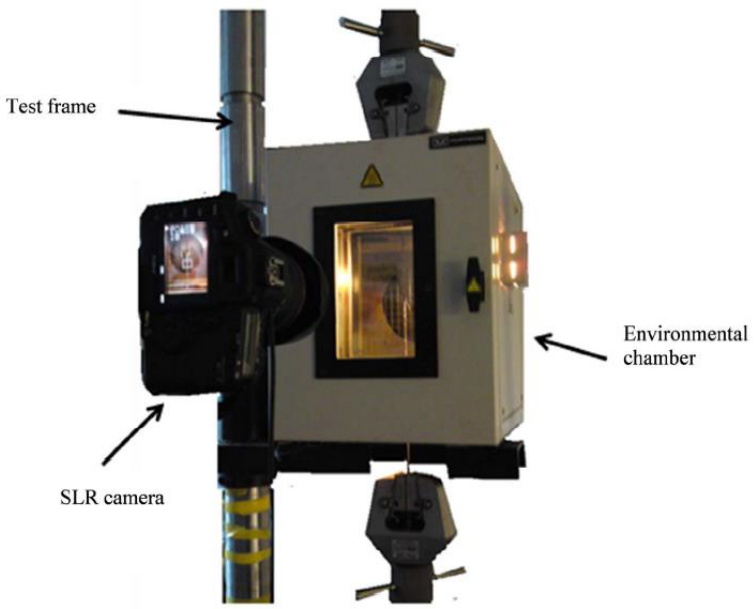

Figure 2: Test setup and digital SLR camera used for optical DIC measurement analysis.

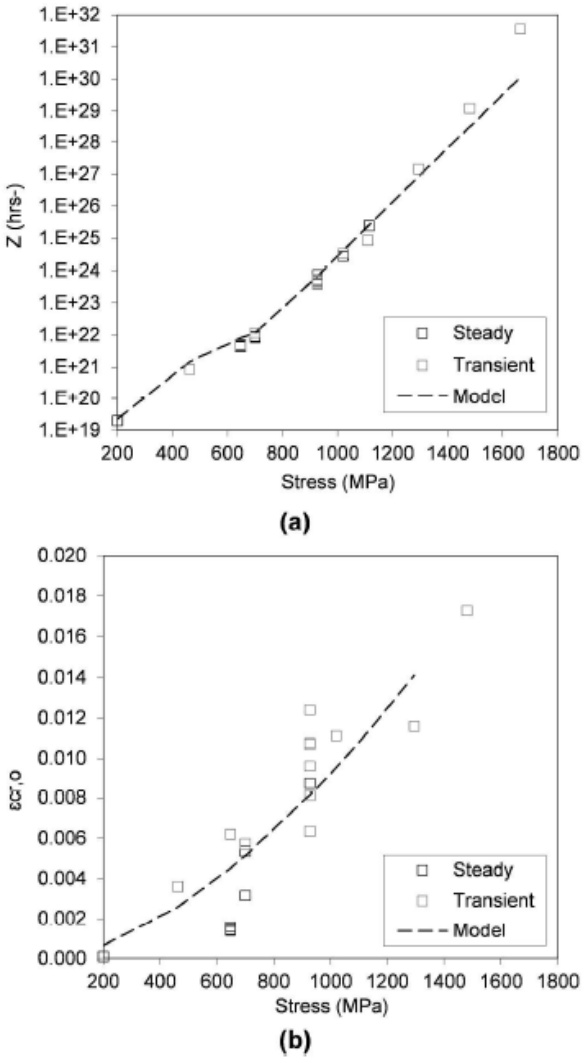

Figure 3: Creep parameters values and Equation 5 predictions for BS 5896 prestressing steel (a) Secondary (b) Primary

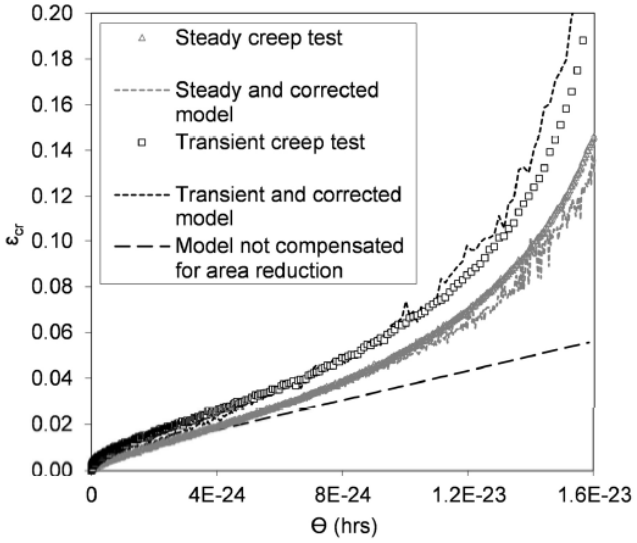

Figure 4: Steady and transient state creep test for BS 5896 prestressing steel at 647 MPa with a posteriori compensated area reduction in modelling prediction.

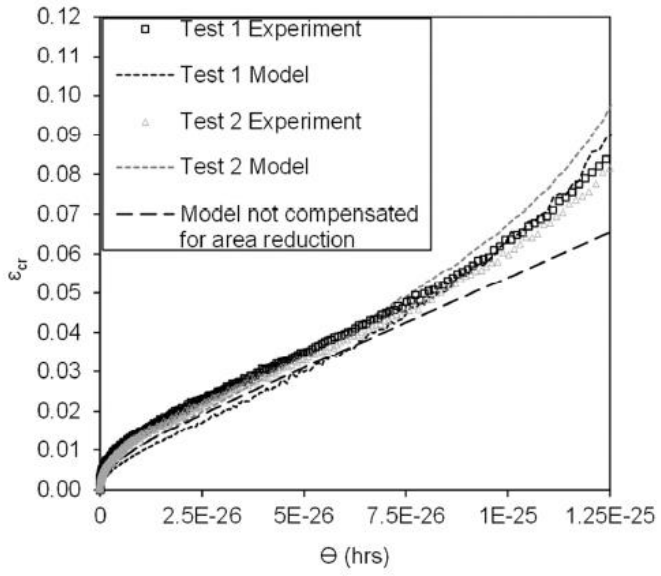

Figure 5: Harmathy model compensated with area reduction for transient state test repeated at 927 MPa

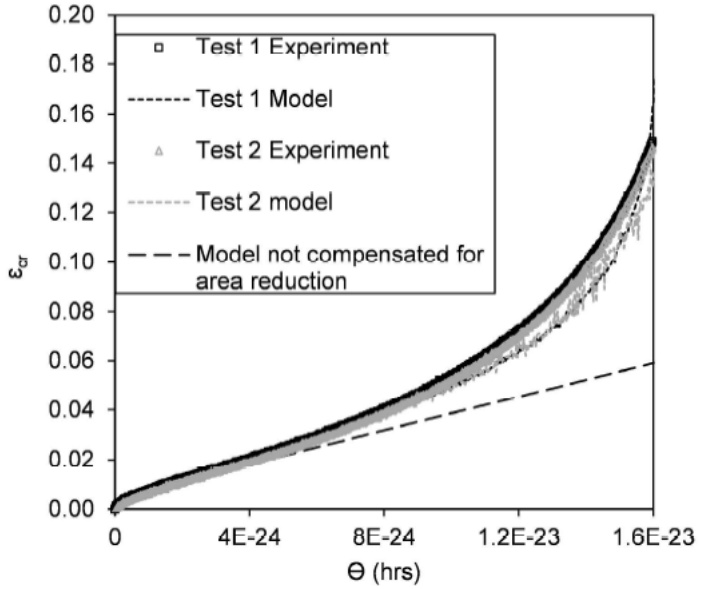

Figure 6: Harmathy model compensated with area reduction for steady state test repeated at 647 MPa

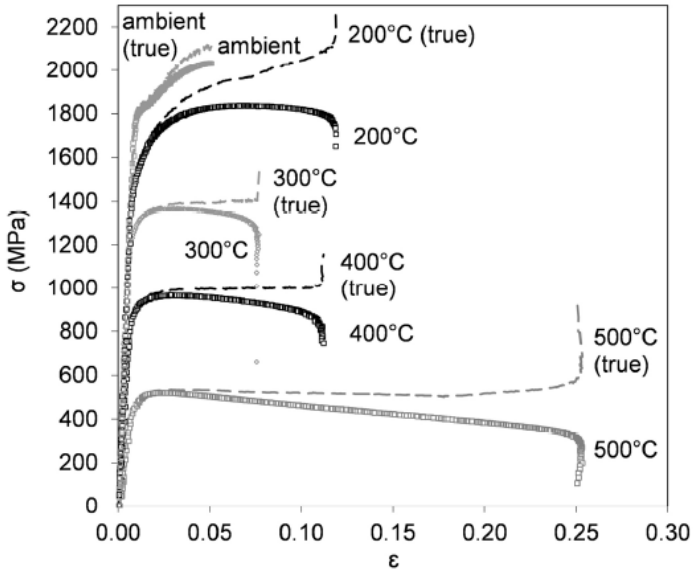

Figure 7: Engineering and true stress versus strain curves for strength tests of BS 5896 prestressing steel.

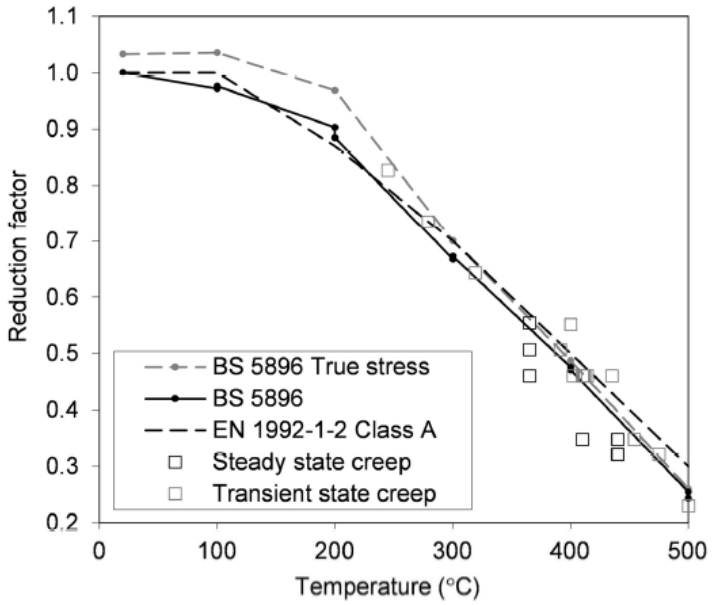

Figure 8: Strength reductions and steady state and transient creep rupture strengths plotted with temperature for BS 5896 prestressing steel.

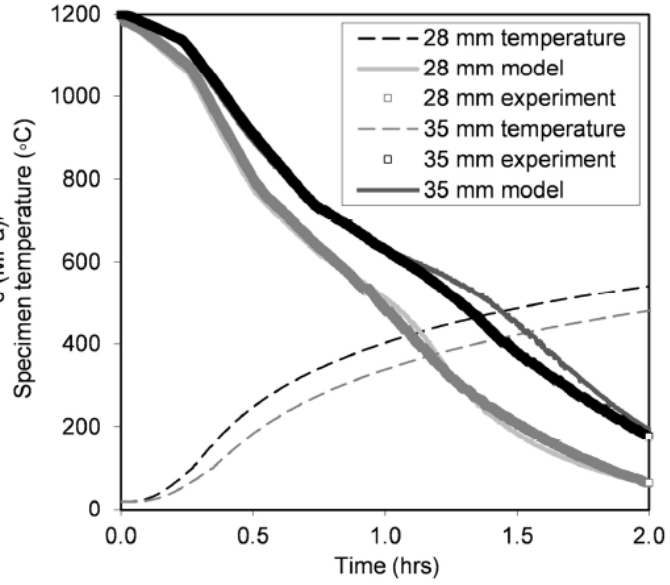

Figure 9: Stress relaxation with simulated standard fire axis distance temperature for BS 5896 prestressing steel.

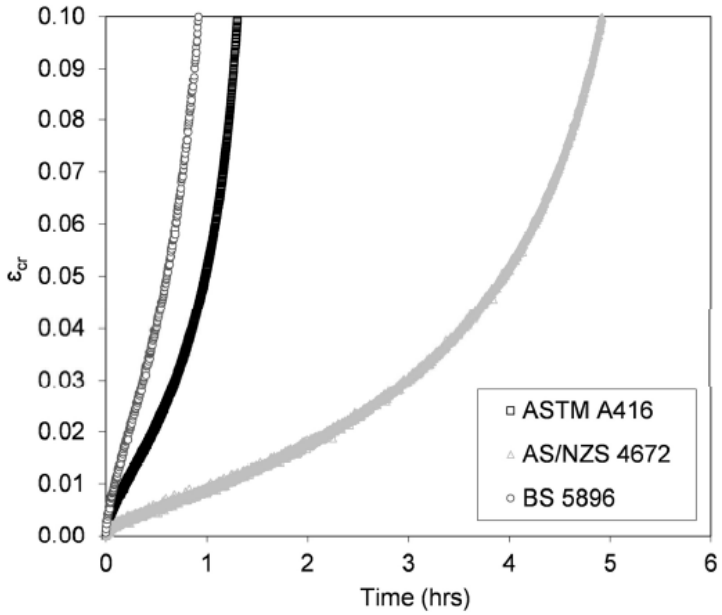

Figure 10: Experimental creep curves for different prestressing steels at 427ºC at 35% ambient temperature fpu.

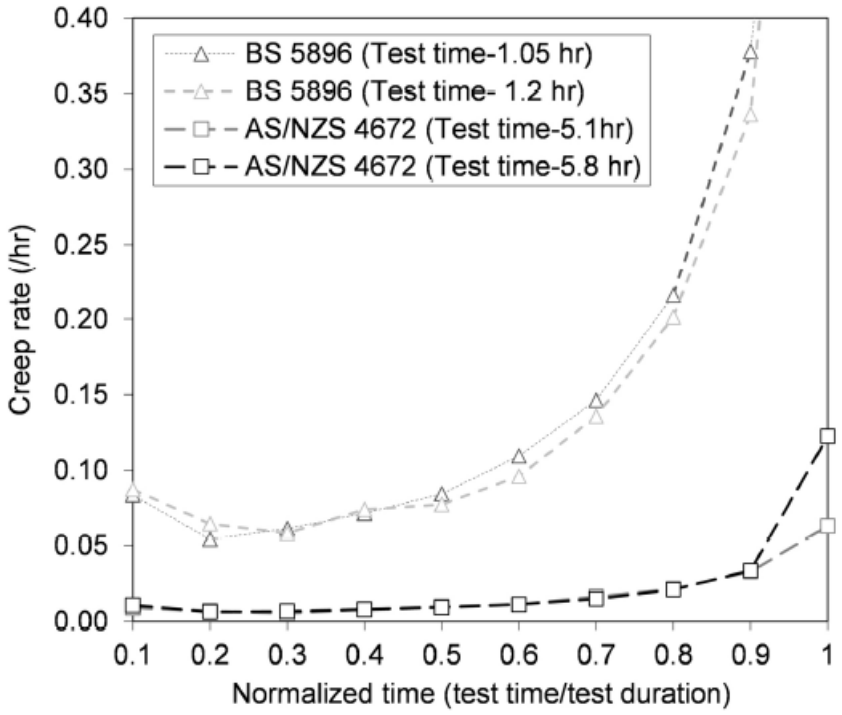

Figure 11: Creep rate with normalized time for BS 5896 and AS/NZS 4672 prestressing steels.

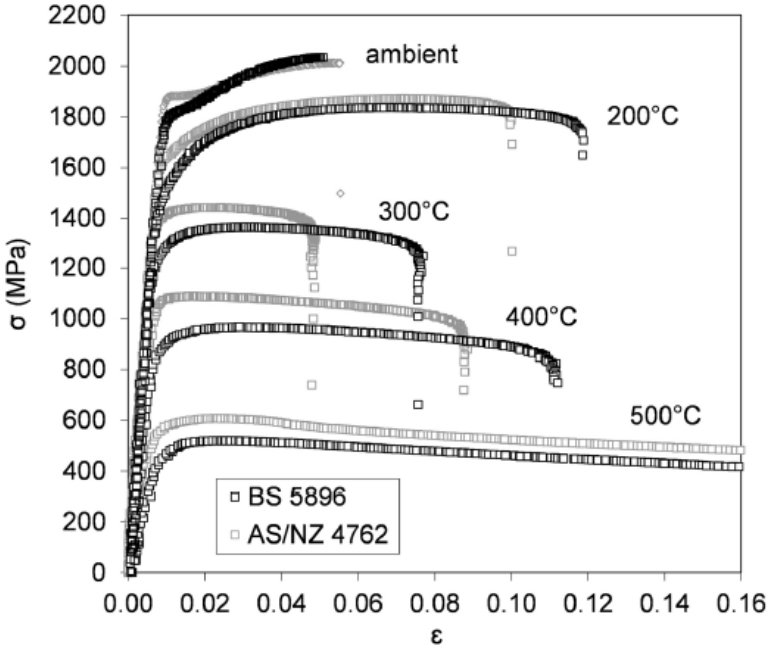

Figure 12: Stress and strain comparison for BS 5896 and AS/NZS 4672 prestressing steels.

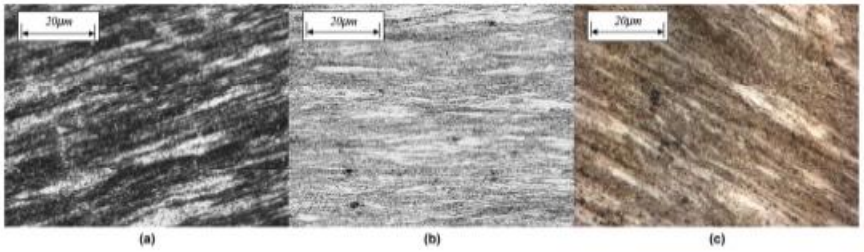

Figure 13: Prestressing steel microstructure for (a) AS/NZ 4672 (b) ASTM A416 (c) BS 5896.

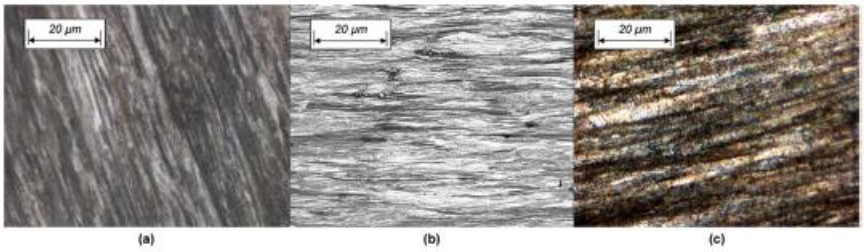

Figure 14: Prestressing steel microstructure after heating at 500ºC for 1.5 hours for (a) AS/NZ 4672 (b) ASTM A416 (c) BS 5896.

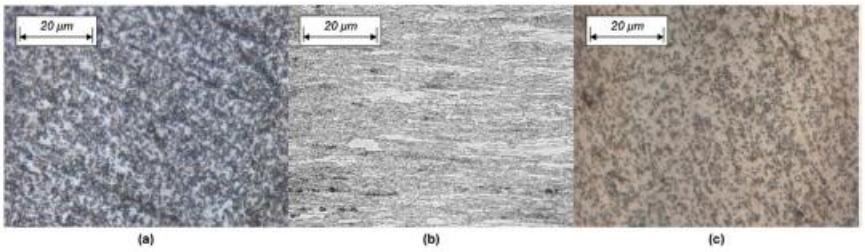

Figure 15: Prestressing steel microstructure after heating at 700ºC for 1.5 hours for (a) AS/NZ 4672 (b) ASTM A416 (c) BS 5896.

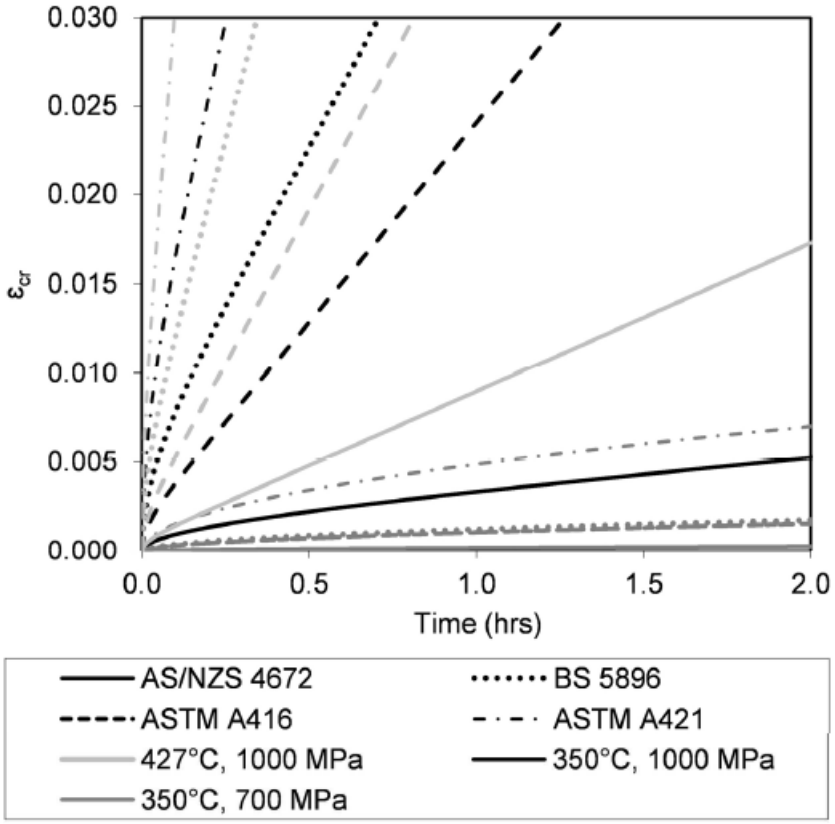

Figure 16: Steady state modelled creep deformation for various heat and load scenarios.

Table 1: Summary of tests

SC- Steady state creep, TC- Transient state creep, CL- Constant load, TE-thermal expansion, S- Strength, SR- Stress Relaxation

a) BS 5896

Test series	Test type	Target stress (MPa)	Target temperature (°C)	Loading (mm/min or °C/min)	# Tests
1a	SC	200	480	-	1
2a	SC	647	440	-	3
3a	SC	700	410	-	1
4a	SC	700	427	-	2
5a	SC	700	440	-	1
6a	SC	927	365	-	1
7a	SC	1115	365	-	1
8a	SC	1200	365	-	1
9a	TC	462	-	2	1
10a	TC	647	-	2	1
11a	TC	700	-	2	1
12a	TC	927	-	1	1
13a	TC	927	-	2	4
14a	TC	927	-	10	1
15a	TC	1020	-	2	1
16a	TC	1110	-	2	1
17a	TC	1294	-	2	1
18a	TC	1480	-	2	1
19a	TC	1664	-	2	1
20a	TE	0	500	10	3
21a	S	-	22-500	1, 2	17
22a	SR	1200	-	variable	2

b) ASTM A416

Test series	Test type	Target stress (MPa)	Target temperature (°C)	Loading (mm/min or °C/min)	# Tests
1b	SC	690	427	-	1
2b	TC	690	-	2	1
3b	TC	800	-	2	1
4b	TC	1000	-	2	2
5b	TC	1000	-	10	1
6b	CL	1000	-	-	1
7b	TE	0	500	10	2
8b	S	-	22,500	2	2

c) AS/NZS 4672

Test series	Test type	Target stress (MPa)	Target temperature (°C)	Loading (mm/min or °C/min)	# Tests
1c	SC	700	427	-	2
2c	SC	700	440	-	1
3c	TC	700	-	2	1
4c	TC	1000	-	2	1
5c	TC	1200	-	2	1
6c	TE	0	500	10	1
7c	S	-	22-500	2	7

Table 2. Chemical composition as a percentage mass of the prestressing steels considered in the current study

Element	BS 5896 [8]	ASTM A416 [9]	AS/NZS 4672 [10]	ASTM A421 [11]
C	0.88	0.80	0.79	0.79
Cr	0.01	0.04	0.29	Not measured
Mn	0.61	0.87	0.59	0.78
P	0.0070	0.023	0.012	0.012
Si	0.26	0.45	0.28	0.19
S	0.019	0.012	0.008	0.031
Ni	0.02	trace	0.03	Not measured
Cu	0.01	trace	0.14	Not measured